Desalination and Water Treatment
www.deswater.com

doi: 10.5004/dwt.2021.26759

215 (2021) 98–107
March

Removal of Cr(VI) from aqueous solutions using montmorillonite-biochar composites

Xiwei Cao[a,*], Xin Zhou[a,*], Mengya Hao[a], Xue Mei[b]

[a]*College of Environmental Science and Engineering, Taiyuan University of Technology, Taiyuan 030024, China, emails: caoxiwei0649@163.com (X. Cao), zhouxin@tyut.edu.cn (X. Zhou), 2630554378@qq.com (M. Hao)*
[b]*School of Civil Engineering, University of Leeds, Woodhouse Lane, LS2 9JT, Leeds, United Kingdom, email: meixue_2018@sina.com*

Received 25 February 2020; Accepted 1 November 2020

ABSTRACT

Montmorillonite, attached to paralyzed biochar, was used to develop novel biochar for removing Cr(VI) from aqueous solution. The biochar feedstock was pyrolyzed at 250°C for 2 h and then stirred with montmorillonite in distilled water. The structure and surface morphology of biochar, montmorillonite, and composite materials were characterized by scanning electron microscopy with energy-dispersive X-ray spectroscopy and transmission electron microscopy. The composite materials inherit the properties from both montmorillonite and biochar. The fitting results of adsorption kinetics and isotherms analysis show that modified biochar is more in line with the pseudo-second-order and Langmuir adsorption model. The maximum adsorption capacity of montmorillonite-modified biochar is 21.75 mg/g. The adsorption effect of SO_4^{2-} and HCO_3^- on the materials is relatively noticeable. The research of this work shows that a modified material with low operational cost and favorable removal efficiency was prepared to remove Cr(VI) from aqueous solution compared with other adsorbents.

Keywords: Engineered biochar; Montmorillonite; Cr(VI); Adsorption

1. Introduction

Heavy metals (Hg, Cd, Pb, Cr, As, etc.) with a density greater than 4.5 g/cm^3 mainly include elements with significant biological toxicity [1], which can cause heavy metal pollution. In recent years, special attention has been paid to heavy metal pollution for non-biodegradable properties and high toxicity. The chromium pollution discharged mostly from textile dying [2] and electroplating [3] industries are one of the significant hazardous contaminants [4]. The concentration of Cr in different wastewater ranges from 5 to 220 mg/L [5], which is much higher than the maximum allowed concentrations by the drinking water (0.05 mg/L), surface water (0.10 mg/L), and wastewater industries (0.25 mg/L), respectively [6]. Trivalent chromium (Cr(III)) and hexavalent chromium (Cr(VI)) existing primarily in nature are two forms of chromium. Cr(VI) with carcinogenicity [7] is much more dangerous than Cr(III) for its toxicity [8]. The main methods to determine the concentration of Cr(VI) in an aqueous medium include spectrophotometry and the electrochemical electrode method. Some novel modified carbon paste electrodes using nanoparticles and an ionic liquid, as well as potentiometric ion-selective electrodes, recently applied which provided advantages such as fast analysis, high selectivity [9,10]. Several efforts can be made to remove Cr(VI) from aqueous solutions, such as reduction, adsorption, extraction, ion exchange, and membrane filtration in some previous studies [11–13].

Nowadays, adsorption as an effective method to remove Cr(VI) has been attracted more attention because of its cost-effectiveness, high efficiency, and easy operation [14–16]. Many kinds of adsorbents, such as carbonaceous, biochar,

* Corresponding authors.

minerals, and nanomaterials [4,17,18], have been proposed. Among these materials, biochar, and minerals (e.g., silica, montmorillonite) have received increasing attention [19,20]. Biochar derived from forest and agricultural residues can be pyrolyzed at low temperature in the oxygen-limited environment [21]. The ability of biochar to remove heavy metals from aqueous media has been verified [22,23]. Compared with other materials such as activation carbon, biochar owns a larger surface area and higher porosity [4] as well as low-cost and good treatment effect. It has a large number of functional surface groups offering potential sites to bind to chromium ions [24–26].

Meanwhile, some researchers have confirmed that clay minerals can stimulate the removal of Cr(VI) due to the chemical and physical properties such as high ion exchange capacity, lamellar structure, and high surface area [27]. Cr(VI) can be reduced with the release and adsorption of Fe(II) in minerals [8,28]. Montmorillonite is one of the common clays whose layers are negatively charged due to the isomorphous replacement of Al^{3+} for Si^{4+} and Mg^{2+} for Al^{3+} in the tetrahedral and octahedral layer [29]. Besides, it has a high cation exchange capacity (CEC) due to the neutralization of the permanent negative charges and cations like Na^{+} and Ca^{2+} [30–32]. Montmorillonite tended to expand easily, which was not suitable to be used directly [28]. The combination of montmorillonite and biochar can take advantage of these two materials to improve the removal efficiency of Cr(VI). Nevertheless, to our best knowledge, a new and improved-functions adsorbent combining these two low-cost adsorptive materials has been barely reported.

Therefore, this study aims to develop a novel preparation method of montmorillonite-biochar composites for efficient removal of Cr(VI) from aqueous solution. The physico-chemical characteristics of this new clay-biochar composites were observed by scanning electron microscopy with energy-dispersive X-ray spectroscopy (SEM-EDS), transmission electron microscopy (TEM), Fourier-transform infrared spectroscopy (FTIR), and Brunauer–Emmett–Teller (BET). The efficiency and mechanisms of Cr(VI) removal from aqueous solution by montmorillonite-biochar composites were investigated under different environmental conditions (e.g., pH, anion, and temperature).

2. Materials and methods

2.1. Chemicals

Montmorillonite, $(Na, Ca)_{0.33}(Al, Mg)_2(Si_4O_{10})(OH)_2{\cdot}nH_2O$, was obtained from Sinopharm Chemical Reagent Co., Ltd. The specific surface area (SSA) of montmorillonite was 20–40 m^2/g. Corn straw collected from the farm was prepared as raw materials of biochar. All the chemicals were analytical reagent grade and achieved from Shanghai Chemical Co., Ltd., China.

2.2. Preparation of biochar and montmorillonite-biochar

The corn straw was washed with deionized water before oven-dried at 60°C. The biomass sample was crushed, ground into powder, put into ceramic crucibles with lids, and heated in a muffle furnace in an oxygen-limited environment at the temperature of 250°C for 2 h. Then, it was cooled at room temperature and sieved through a 0.15 mm mesh. The pristine biochar was obtained.

30 g biochar powder and 30 g montmorillonite were added to 500 mL distilled water and stirred for 2 h to prepare a stable suspension. The composites were centrifuged, dried at 105°C and filtered with a 0.15 mm sieve. The pristine biochar, montmorillonite, and clay-modified biochar were referred to as biochar (BC), montmorillonite (MMT), and BC-MMT, respectively.

2.3. Sample characterization

The surface area and pore size of the three samples were measured by NOVA 4200e surface area and pore size analyzer (Micromeritics, Empyrean, USA) at a relative pressure of 0.95. The surface structure and morphology of BC, MMT, and BC-MMT were characterized by the scanning electron microscope with energy-dispersive X-ray spectrometer (SEM-EDS, JEOL, JSM-6360LV, Japan; OXFORD, X-act) and transmission electron microscope (TEM, JEOL, JEM-1011, Japan). The materials were recorded between 400 and 4,000 cm^{-1} by a Nexus 670 FTIR spectrometer (Thermo Nicolet, Madison).

2.4. Cr(VI) removal experiments

BC, MMT, and BC-MMT (0.2g for each) were added separately in 25 mg/L Cr(VI) aqueous solution at pH 2.0. The flasks were placed in a shaking bath at 30°C and mixed at 150 rpm for 100 min with the time intervals of 5, 10, 15, 20, 30, 40, 60, 80, and 100 min. A 1 mL sample was taken from the shaker and immediately filtered through a 0.45 μm pore size filter membrane at regular intervals to determine the Cr(VI) concentrations in an aqueous solution. The concentration of Cr(VI) ions was recorded by the 1,5-diphenylcarbohydrazide spectrophotometric method using a UV-visible spectrophotometer (λ_{max} = 540 nm). All experiments were repeated three times. The data difference was less than 5%. The averages were reported.

The effects of pH on the removal of Cr(VI) by BC-MMT were studied under the pH condition at 1, 2, 3, 13, and 14, respectively. The pH values were adjusted by adding small aliquots of 0.1–1.0 mol/L NaOH/HCl. The other steps were the same as the kinetic removal experiments. Besides, FTIR was used to characterize the functional groups of BC-MMT at a pH of 1, 7, and 14.

Adsorption isotherm of Cr(VI) on BC-MMT was examined with 50 mg/L Cr(VI) aqueous solution and different dosages of montmorillonite-biochar composites ranging from 0.05 to 0.4 g at the temperature of 20°C, 30°C and 40°C for 3 h when pH was 2.0. Furthermore, 25 mg/L Cr(VI) was mixed with different concentrations of salt ions (SO_4^{2-}, HCO_3^-) from 0 to 8 mmol/L to measure the effect of the ions at pH 2.0. SO_4^{2-} and HCO_3^- of different concentrations were only added in the experiment of the effect of anions.

2.5. Data analysis

The amount of Cr(VI) adsorbed on the materials at equilibrium, q_e (mg/g), was calculated by Eq. (1) below:

$$q_e = \left(C_0 - C_e\right)\frac{V}{m} \quad (1)$$

For the removal experiments, *R*%, the removal efficiency was determined as follows:

$$R\% = \frac{C_0 - C_e}{C_0} \times 100\% \quad (2)$$

where C_0 represents the initial Cr(VI) concentration (mg/L); C_e represents the concentration in the filtered aqueous solution; V is the volume (mL) of the suspension and m is the mass (g) of the adsorbent.

3. Results and discussion

3.1. Characterization of BC-MMT

The distribution and morphology of BC, MMT, and BC-MMT were characterized by SEM images. The EDS spectrum was carried out to analyze the surface structure of these three materials. Fig. 1a clearly shows the side of a tubular structure of BC, which is consistent with other literature that paralyzed straw is a porous material with tunneling structure inside [33]. After zooming at 10,000× magnification, the surface of BC is generally large and smooth. Some debris particles are attached on the biochar surface. According to the characteristics of BC morphology, BC is proved to be an excellent support material to host the distribution of MMT.

Montmorillonite consists of two tetrahedrons and one octahedral unit which forms a sheet of about 1 nm. It has expandable-layered silicates [34]. The montmorillonite surface presents the structure of a thin-film (Fig. 1b), a common structure of clay minerals [35,36]. The rough surface of MMT can increase the adsorption area further. MMT particles have a non-uniform size and tend to expand easily, which may make it difficult to apply to the actual application directly. Fe(II) is a common substitute in MMT. Al(III) in montmorillonite can be replaced by Fe(II), leading to the negative charged of montmorillonite, which is consistent with the result that oxygen, silicon, iron, calcium, aluminum, magnesium are detected in Fig. 2b [34]. Furthermore, the Fe(II) can reduce Cr(VI) to Cr(III), which is beneficial to the removal of Cr(VI) (Fig. 3) [8].

As shown in Fig. 1c, the BC-MMT surface is rough while the BC surface is smooth. Few aggregates can be seen on the surface of BC-MMT, illustrating that MMT has been successfully attached to the biochar surface. The modification of BC with MMT can increase the surface area of the adsorbent. Carbon, oxygen, silicon, iron, calcium, aluminum, and magnesium are detected in BC-MMT (Fig. 2c). As oxygen and carbon are the typical elements in biochar and silicon, iron, calcium, aluminum, magnesium are the main elements in MMT, the result of this spectrum shows that MMT and BC are in BC-MMT.

TEM is carried out to further analyze the morphology of the three materials. The edge of the biochar is clear, and it shows the porous structure with a smooth surface (Fig. 1d). The release of volatile components facilitates the generation of the tunneling structure and the smooth surface of BC. As can be seen in Fig. 1e, the TEM edge of MMT is not clear, and the shape of MMT is irregular compared with that of biochar. Fig. 1f shows that the BC-MMT boundary also appears to be dispersed, meaning that montmorillonite is successfully attached to the surface of biochar.

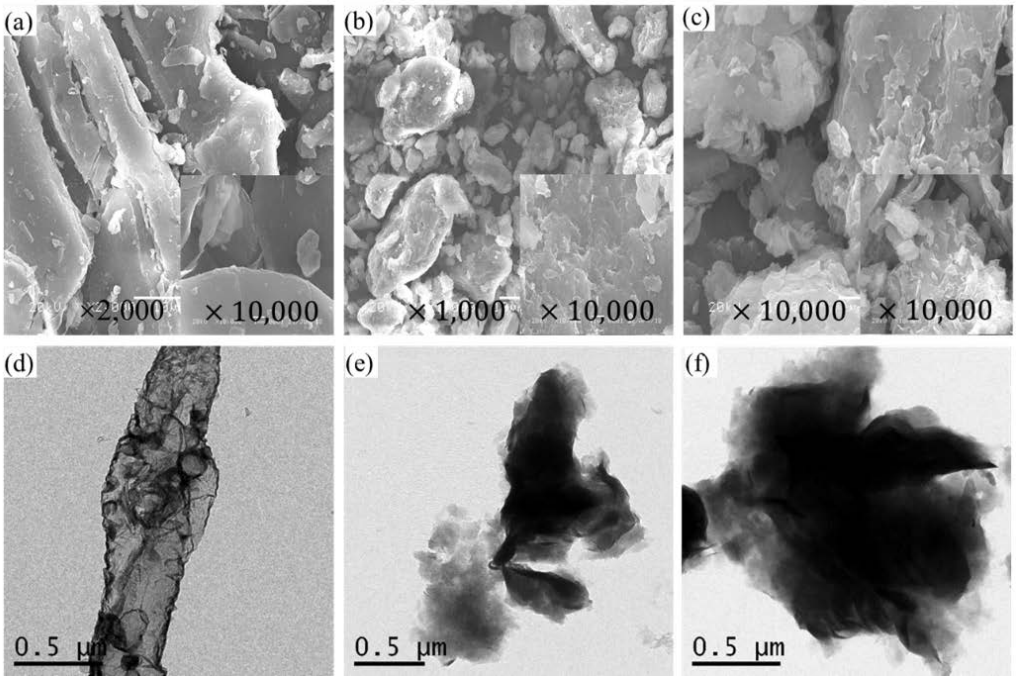

Fig. 1. Scanning electron microscopy images of (a) BC, (b) MMT, (c) BC-MMT and BC-MMT-Cr; transmission electron microscopy images of (d) BC, (e) MMT, (f) BC-MMT.

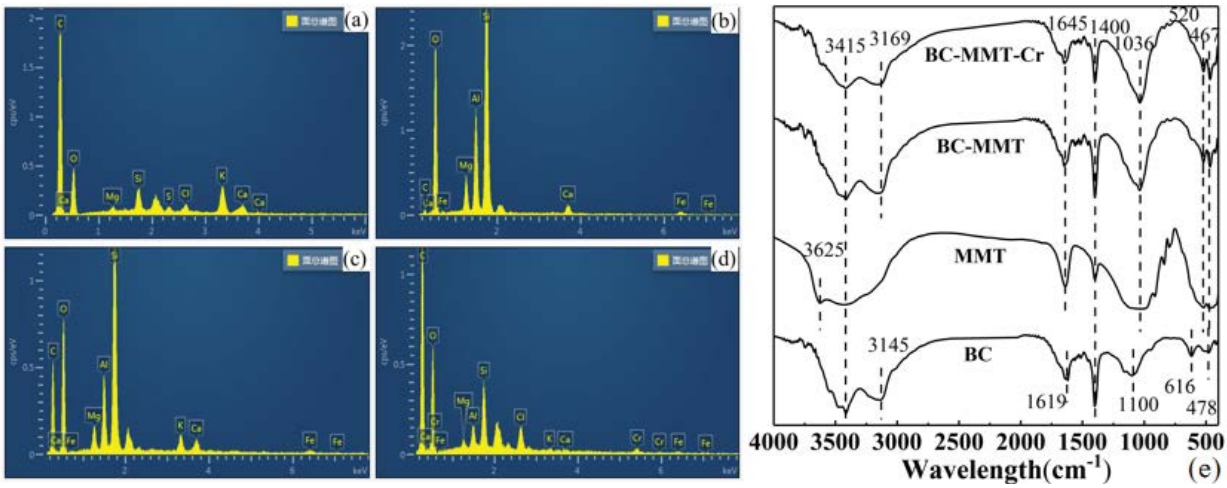

Fig. 2. Energy-dispersive X-ray spectrum of (a) BC, (b) MMT, (c) BC-MMT, (d) BC-MMT-Cr, (e) Fourier-transform infrared spectrum of BC, MMT, BC-MMT, and BC-MMT-Cr.

After the reaction with Cr(VI), the adsorbent surface is rougher and a clear clay film is noticed on the BC-MMT surface. By comparing Figs. 2c and d, the content of Cr(VI) is detected on the surface of the adsorbent material. It can be preliminarily determined that the kind of material can adsorb Cr(VI) from aqueous solutions.

In Fig. 2, the value of 3,415 cm^{-1} is mostly related to –O–H stretch, implying hydrogen-bonding interactions. The broadband centers at 3,145 cm^{-1}, which is caused by –C=CH [28]. The spectrum is included the band at 1,619 cm^{-1}, in the range of 1,650–1,600 cm^{-1}, which is assigned as C=C skeletal vibration bands and aromatic C=O groups [37]. The peaks at 1,401 and 1,100 cm^{-1} suggest the presence of –COOH and –Si–O, respectively. The existence of –OH and –COOH can enhance the absorptive ability of the material to hexavalent chromium via ion exchange (Fig. 3). Strong absorption peaks are detected according to the FTIR pattern of the MMT sample, corresponding to the peak of Fe–O (519 cm^{-1}) and the peak of Si–O–Si (468 cm^{-1}). It includes a band at 3,625 cm^{-1}, which is assigned as –NH. The result from the FTIR spectra of BC-MMT is similar to that of BC, but there is more Fe–O (520 cm^{-1}), –Si–O–Si (467 cm^{-1}) functional groups [38], indicating that MMT is successfully attached on the BC surface. Furthermore, the increase of oxygen groups in BC-MMT is beneficial to remove the Cr(VI) ions from an aqueous solution [28].

The structural characteristics of BC-MMT were obtained by the adsorption–desorption isotherms of N_2 (Fig. 4). According to the Brunauer–Deming–Deming–Teller classification, the N_2 adsorption–desorption isotherms of both MMT and BC-MMT samples are of classical type IV. Therefore, both samples are classified as mesoporous material. The average pore size, the Barrett–Joyner–Halenda (BJH) total pore volume, and the BET surface area of BC-MMT are 18.05 nm, 0.017 m^2/g, and 1.76 m^2/g, respectively. Although the BET surface area (31.30 m^2/g) and the BJH total pore volume (0.096 m^2/g) of MMT are larger than those of BC-MMT, the average pore size of the montmorillonite is only 9.33 nm, which is 51.69% of the average pore size of BC-MMT. The *t*-plot external surface area and the *t*-plot micropore area of MMT are 26.83 m^2/g and 4.47 m^2/g, accounting for 85.7% and 14.3% of the total surface area, respectively. The external surface area of the MMT is much larger than its internal micropore area. Due to the adhesion of MMT to the surface of BC, the average pore size of BC-MMT increases [28], which improves the adsorption capacity to water pollutants significantly.

3.2. Adsorption kinetics

The kinetic study is carried out to describe the adsorption efficiency of three kinds of materials, and the data of the adsorption process is fitted. As shown in Fig. 5, the removal efficiency of BC, MMT, BC-MMT reaches 87.63%, 5.54%, and 84.18% after 100 min reaction, respectively. The removal efficiency of Cr(VI) from water by montmorillonite is much lower than that by BC and BC-MMT due to the cluster of MMT. Though it is reported that montmorillonite has shown a relatively high CEC [30], MMT as an adsorbent material is unsuitable for removing Cr(VI) alone. It is shown that the removal efficiency of BC is slightly higher than that of BC-MMT after 100 min reaction. However, BC-MMT consists of 50% BC and 50% MMT. The removal efficiency of BC-MMT is higher than the simple addition of BC and MMT.

The adsorption efficiency of BC, MMT, and BC-MMT is analyzed by kinetics as shown in Fig. 5. The experimental data are fitted by following pseudo-first-order, pseudo-second-order, Elovich and intraparticle diffusion models [39–41]:

$$\ln\left(q_e - q_t\right) = \ln q_e - k_1 t \tag{3}$$

$$\frac{t}{q_t} = \frac{1}{k_2 q_e^2} + \frac{t}{q_e} \tag{4}$$

$$q_t = \frac{1}{\omega}\ln\left(\alpha\omega\right) + \frac{1}{\omega}\ln t \tag{5}$$

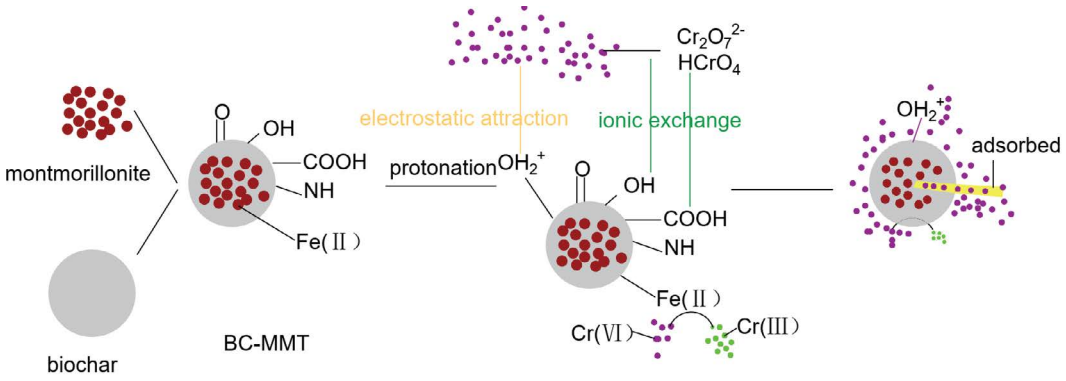

Fig. 3. Removal mechanism of Cr(VI) by BC-MMT [28].

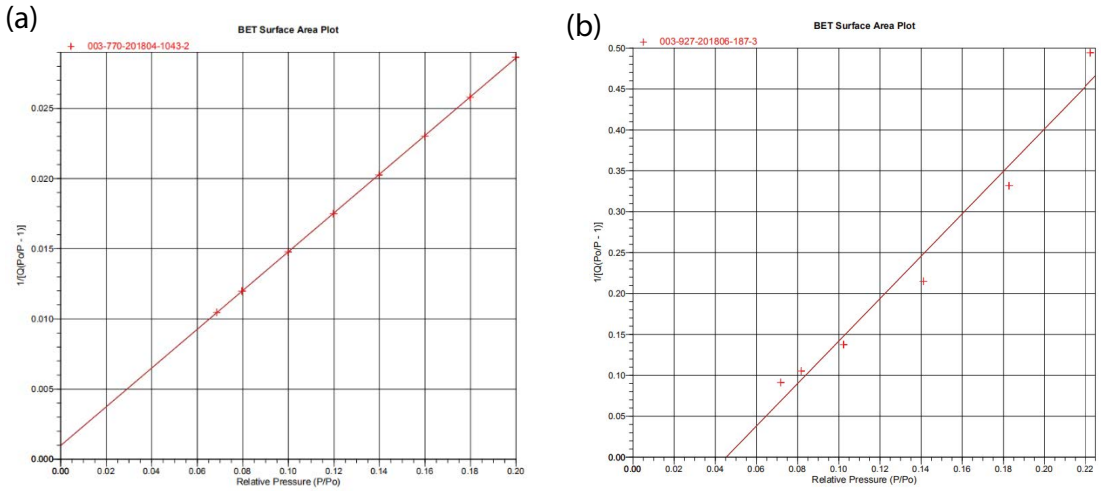

Fig. 4. Brunauer–Emmett–Teller analysis of (a) MMT and (b) BC-MMT.

$$q_t = k_i \cdot t^{1/2} + I \tag{6}$$

where q_t represents the amount of Cr(VI) absorbed at time t; q_e means the amount of Cr(VI) absorbed at equilibrium; k_1, k_2, and k_i are adsorption rate constants; α is the initial adsorption rate; ω is the desorption value; I is an index for the thickness of the boundary layer.

The fitting results of adsorption kinetics are shown in Fig. 5, and the corresponding fitting parameters are illustrated in Table 1. The R^2 value obtained by pseudo-second-order kinetics is closer to 1 than the R^2 values obtained by pseudo-first-order kinetics and Elovich models. The q_e calculated by pseudo-second-order kinetics is close to the experimental data. Thus, pseudo-second-order kinetics can fit the adsorption process of Cr(VI) by BC and BC-MMT better, indicating that the adsorption of Cr(VI) by the adsorption materials is mainly controlled by the chemical adsorption and new chemical substances are formed on the surface of the adsorbent [42,43]. Furthermore, according to the result of pseudo-second-order kinetics, BC-MMT has a higher adsorption capacity for Cr(VI) compared to BC. Besides, according to Fig. 5f of the intraparticle diffusion models, the adsorption process can be divided into two stages. The rapid adsorption stage is the penetration of chromium(VI) through a thin water film around the adsorbent. In the slow stage, the pollutant penetrates into the adsorbent particles, which limits the reaction speed [40]. Thus, this way can be considered a potential method to take advantage of both biochar and MMT to remove heavy metals from aqueous solutions. Furthermore, the amount of Cr(VI) absorbed at equilibrium is higher than that in a similar study [28], indicating that this material is successfully developed.

3.3. Effect of initial pH

pH is a significant factor influencing the removal of pollutants by adsorbents in aqueous solutions. The adsorption of Cr(VI) was investigated at different pH values. In Fig. 6, the adsorption of Cr(VI) decreases gradually with the increase of pH value in acidic solutions. The equilibrium removal efficiency of Cr(VI) by BC-MMT at pH of 1, 2, and 3 is 100.0%, 84.18%, and 19.28%, respectively. With the decrease of the pH in the solution, more functional groups on the surface of the BC-MMT are protonated [44,45], and more positive charges appear on the surface of the composite. The common species of Cr(VI) exist in the form of $HCrO_4^-$, CrO_4^{2-}, $Cr_2O_7^{2-}$ in solution. The positive charge on the surface of the adsorption material can attract Cr(VI) anions in an aqueous solution, which increases the

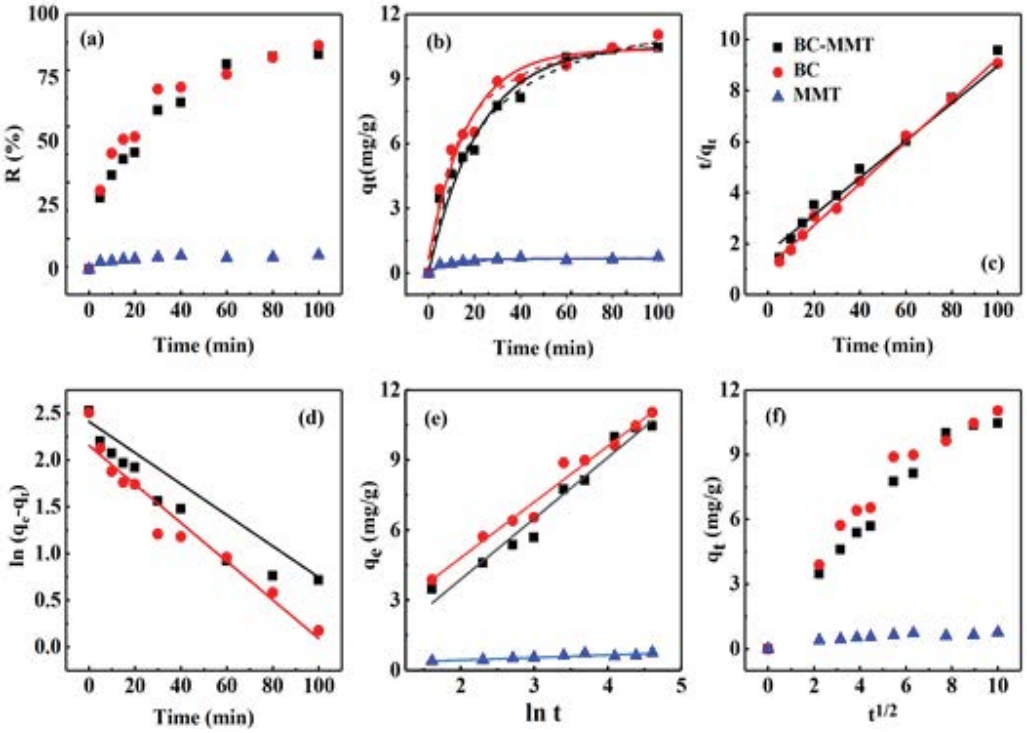

Fig. 5. Kinetic models for Cr(VI) adsorption using BC, MMT and BC-MMT: (a) adsorption data, (b) non-linear fitting of pseudo-first-order (full line) and pseudo-second-order (line of dashes), (c) linear fitting of pseudo-second-order, (d) linear fitting of pseudo-first-order, (e) linear fitting of Elovich, and (f) intraparticle diffusion model.

Table 1
Comparison of kinetic parameters for adsorption

Model	Parameter	BC	MMT	BC-MMT
Pseudo-first-order	q_e (mg/g)	8.61	0.33	9.63
	k_1 (min^{-1})	0.021	0.0219	0.018
	R^2	0.939	0.392	0.926
Pseudo-second-order	q_e (mg/g)	12.23	0.75	12.50
	k_2 (min^{-1})	0.0061	0.209	0.0044
	R^2	0.995	0.976	0.989
Elovich	q_e (mg/g)	7.03	4.94	5.90
	α (mg/g·min)	2.43	0.86	1.57
	ω (g/mg)	0.42	9.22	0.38
	R^2	0.977	0.810	0.969
Intraparticle diffusion	k_i (mg/g/min$^{1/2}$)	1.045	0.06	1.07
	I	1.69	0.211	0.99
	R^2	0.912	0.718	0.956

removal efficiency of Cr(VI). The adsorption of Cr(VI) from the wastewater was negligible at pH = 4–12. With the increase of pH value from pH 13 to 14, the removal efficiency was increased from 46.26% to 82.50%.

Besides, the experimental data of BC-MMT for Cr(VI) are fitted by pseudo-first-order and pseudo-second-order model, respectively. By comparing the parameters in Table 2, the adsorption of Cr(VI) by BC-MMT in different pH is closer to the pseudo-second-order, which implies the primary process is chemisorption.

FTIR is carried out to further illustrate the changes in functional groups of BC-MMT at different pH levels. For BC-MMT at pH of 7, the peaks of 3,415 cm^{-1} assigned to –OH, 3,160 cm^{-1} assigned to –C=CH, 1,645 cm^{-1} assigned to –C=O, 1,401 cm^{-1} assigned as –COOH, 1,037 cm^{-1} assigned to –Si–O, 520 cm^{-1} assigned to Fe–O and 467 cm^{-1} assigned to Si–O–Si appear. The intensity of –OH at 3,415 cm^{-1} and –C=CH at 3,160 cm^{-1} is markedly weakened when pH value is 1 and 14, indicating a possible interaction in acidic or alkaline solutions [28]. As shown in Fig. 3, in acid conditions,

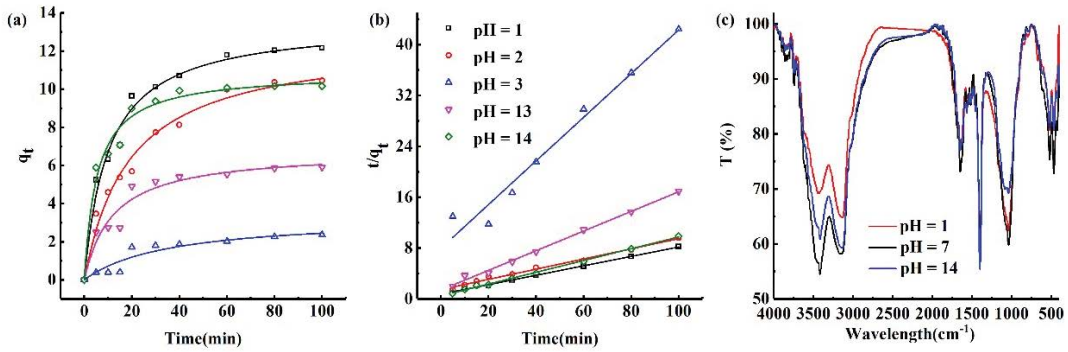

Fig. 6. Effect of pH on the removal of Cr(VI) by BC-MMT: (a) non-linear fitting of pseudo-second-order, (b) linear fitting of pseudo-second-order, and (c) Fourier-transform infrared spectrum of BC-MMT at pH 1, 7 and 14.

Table 2
Comparison of parameters for Cr(VI) removal in different pH

	Pseudo-first-order			Pseudo-second-order		
	q_e (mg/g)	k_1 (min^{-1})	R^2	q_e (mg/g)	k_2 (min^{-1})	R^2
pH = 1	8.38	0.022	0.866	13.50	0.0074	0.997
pH = 2	9.63	0.018	0.926	12.50	0.0044	0.989
pH = 3	2.49	0.017	0.851	2.91	0.0169	0.965
pH = 13	4.04	0.023	0.750	6.47	0.0172	0.995
pH = 14	4.80	0.026	0.899	10.79	0.0182	0.998

–OH is more possible to be protonated resulting in a positive charge on the surface of the adsorbent, which facilitates the adsorption of chromium-containing anions by electrostatic interaction when pH value is 1 [46–48].

3.4. Adsorption isotherms

The relationship between the adsorbed Cr(VI) by BC-MMT and the Cr(VI) concentration in aqueous solution is described by the adsorption isotherm. In Fig. 7, the amount of adsorbed Cr(VI) increases with the increase of the Cr(VI) ions concentration in the aqueous solution. Furthermore, the adsorbed amount of Cr(VI) increases with the increase of temperature from 20°C to 40°C at the same equilibrium concentration in solution. It shows that the increase in temperature can promote the removal efficiency of Cr(VI). However, as shown in Table 3, the adsorption capacity did not change significantly with temperature.

The experimental data are fitted with Langmuir and Freundlich models shown below to indicate the adsorption mechanism of BC-MMT further.

$$\frac{C_e}{q_e} = \frac{K_L}{q_{\max}} + \frac{C_e}{q_{\max}} \tag{7}$$

$$\ln q_e = \ln K_F + \frac{1}{n}\ln C_e \tag{8}$$

where C_e is the adsorption concentration at equilibrium; q_e and $q_{\max}$ are equilibrium adsorption amount and maximum adsorption amount, respectively; K_L and K_F represent the Langmuir constant and the Freundlich constant, respectively; $1/n$ represents the heterogeneity factor. The fitting parameters for the two models are shown in Table 3.

The R^2 value of the Langmuir model is better than that of the Freundlich model, so the adsorption of Cr(VI) by BC-MMT in solution is closer to the Langmuir form, indicating that adsorption mainly occurs in monolayers. No interaction is found between absorbed metal cations and the surface of BC-MMT has a limited number of active sites [41]. It can be seen from Fig. 7 that, q_e increases with the increase of C_e. The increasing rate slows down gradually, suggesting that as the equilibrium concentration of Cr(VI) increases, the active site is gradually occupied [49]. Meanwhile, as shown in Table 4, the maximum adsorption amount calculated with the Langmuir model for BC-MMT has certain advantages over other similar materials.

3.5. Effect of anions

SO_4^{2-} and HCO_3^- as the common co-existing anions in the discharge of acid mine drainage containing Cr(VI) [28] were selected to explore the effect of anions. Fig. 8 shows the effect of different concentrations of SO_4^{2-} and HCO_3^- on the removal of Cr(VI) from aqueous solutions by BC-MMT. When the concentration of SO_4^{2-} is 0, 2, 4, 6, and 8 mmol/L, the removal efficiency of Cr(VI) by BC-MMT is 84.18%, 55.73%, 54.28%, 51.91%, and 47.14%, respectively. With the increase of SO_4^{2-} concentration in aqueous solution, the removal efficiency of Cr(VI) by adsorbents decreases gradually. SO_4^{2-} hinders the removal of Cr(VI). The surface

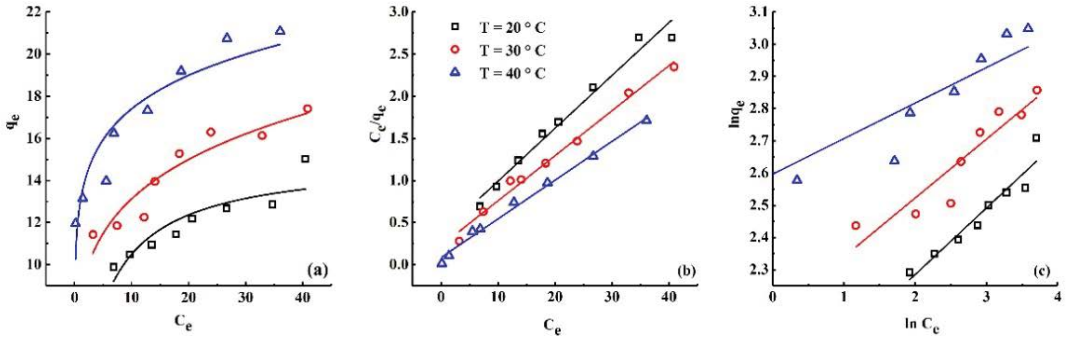

Fig. 7. Effect of temperature on the removal of Cr(VI) by BC-MMT: (a) non-linear fitting of Langmuir adsorption model, (b) linear fitting of Langmuir adsorption model, and (c) linear fitting of Freundlich adsorption model.

Table 3
Comparison of parameters for Cr(VI) removal by different isotherm equations

T	Langmuir adsorption model			Freundlich adsorption model		
	q_m (mg/g)	K_L (L/mg)	R^2	K_F	$1/n$	R^2
20°C	15.93	5.789	0.973	6.50	0.207	0.909
30°C	18.69	4.172	0.987	8.64	0.183	0.850
40°C	21.75	1.829	0.991	13.42	0.110	0.840

Table 4
Comparison of Cr(VI) adsorption capacities of BC-MMT with other adsorbents

Adsorbent	Adsorption capacity (mg g^{-1})	References
Montmorillonite + biochar of peanut shell	18.05	[28]
Biochar prepared by *Ziziphus spina-christi* leaf	13.81	[50]
Montmorillonite + Biochar of corn straw	21.75	This experiment

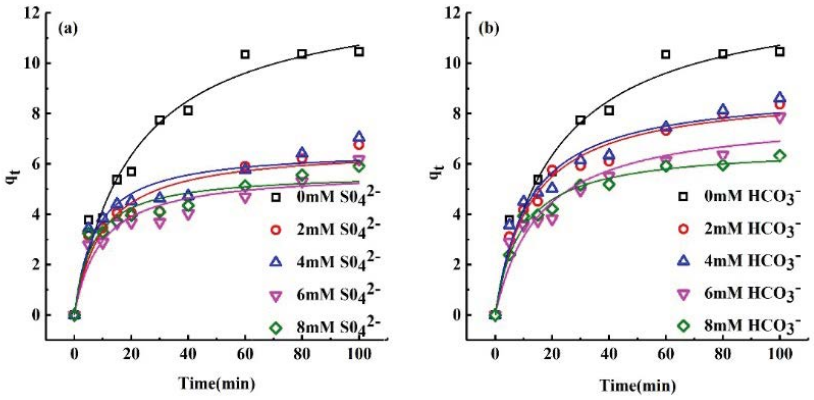

Fig. 8. Effect of anions on the removal of Cr(VI) by BC-MMT.

functional groups of BC-MMT are protonated at a pH value of 2. With the increase of SO_4^{2-} concentration, the competition between SO_4^{2-} and $Cr_2O_7^{2-}$, $HCrO_4^{2-}$ for BC-MMT surface reaction point increases gradually. The q_e value decreases with the increase of SO_4^{2-} concentration in Table 5. The inhibitory effect of SO_4^{2-} on BC-MMT is proved.

Compared to the removal of Cr(VI) without HCO_3^-, HCO_3^- shows an inhibitory effect on the removal efficiency of BC-MMT. With the 8.0 mmol/L HCO_3^-, the removal efficiency and equilibrium adsorption capacity of BC-MMT are 48.32% and 6.68 mg/g, much lower than in the control group (83.15%, 12.93 mg/g) without any HCO_3^-. It is speculated that

Table 5
Comparison of parameters for Cr(VI) removal at different anion concentrations

SO_4^{2-}, (mmol/L)	q_e (mg/g)	k_2 (min^{-1})	R^2	HCO_3^-, (mmol/L)	q_e (mg/g)	k_2 (min^{-1})	R^2
0	12.93	0.004	0.970	0	12.93	0.004	0.970
2	6.67	0.015	0.904	2	8.911	0.009	0.972
4	6.58	0.021	0.906	4	8.967	0.010	0.956
6	5.72	0.019	0.886	6	7.978	0.008	0.927
8	5.65	0.027	0.917	8	6.684	0.016	0.984

the addition of HCO_3^- increases the pH of the aqueous solution, thus reducing the removal efficiency of Cr(VI).

When SO_4^{2-} and HCO_3^- concentration is 8 mmol/L, the equilibrium adsorption amount is 5.65 mg/g and 6.68 mg/g, respectively. The inhibitory effect of HCO_3^- on the adsorption process is not as strong as that of SO_4^{2-} on Cr(VI) removal at the same concentration. HCO_3^- also occupies protons on the surface of BC-MMT. At the same concentration, the protons occupied by HCO_3^- are less than those occupied by SO_4^{2-} and HCO_3^- have less competition with Cr(VI) ions. Thus, there is less effect on Cr(VI) removal.

3.6. Desorption and reusability study

In order to explore the desorption and reusability of BC-MMT, 1 M NaOH was used as the desorbing agent. As shown in Fig. 9, there was no significant decrease in the adsorption capacities of BC-MMT during 8 cycles of adsorption–desorption, indicating that BC-MMT had excellent reusability.

4. Conclusions

A novel engineered biochar with montmorillonite implanted on the paralyzed biochar surfaces was fabricated. The material physicochemical properties of the modified biochar were characterized. Pseudo-second-order and Langmuir adsorption isotherm models can fit the adsorption process well. The maximum adsorption amount of BC-MMT is 21.75 mg/g. The adsorption efficiency can be improved by adjusting pH and temperature. BC-MMT can serve as an efficient, low-cost material for Cr(VI) removal from wastewater with great potentials in a large-scale application.

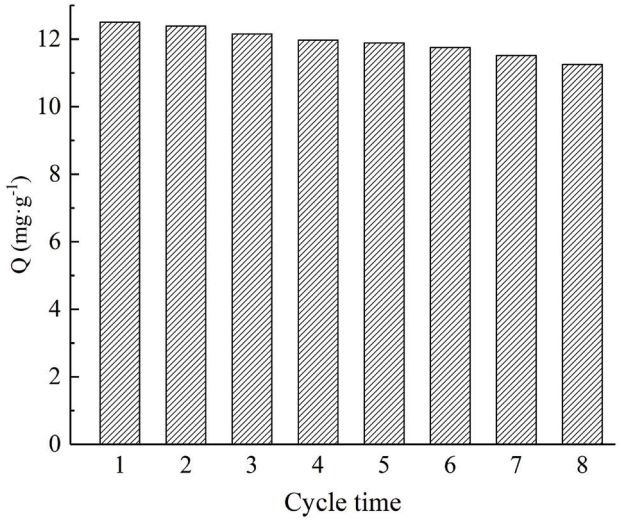

Fig. 9. Adsorption capacity of BC-MMT for Cr(VI).

References

[1] S. Tasharrofi, S. Sadegh Hassani, H. Taghdisian, Z. Sobat, Chapter 24 – Environmentally Friendly Stabilized nZVI-Composite for Removal of Heavy Metals, C.M. Hussain, A.K. Mishra, Eds., New Polymer Nanocomposites for Environmental Remediation, Elsevier, Amsterdam, Netherlands, 2018, pp. 623–642.
[2] P. Thiravetyan, P. Suksabye, Treatment of chromium contamination in the environment, Mater. Sci. Res. J., 5 (2011) 147–183.
[3] Y. Abshirini, H. Esmaeili, R. Foroutan, Enhancement removal of Cr(VI) ion using magnetically modified MgO nanoparticles, Mater. Res. Express, 6 (2019) 1–15.
[4] N. Zhao, Z. Yin, F. Liu, M.Y. Zhang, Y.Z. Lv, Z.P. Hao, G. Pan, J. Zhang, Environmentally persistent free radicals mediated removal of Cr(VI) from highly saline water by corn straw biochars, Bioresour. Technol., 260 (2018) 294–301.
[5] Y. Wang, D.F. Liu, J.B. Lu, J. Huang, Enhanced adsorption of hexavalent chromium from aqueous solutions on facilely synthesized mesoporous iron–zirconium bimetal oxide, Colloids Surf., A, 481 (2015) 133–142.
[6] Q.-Q. Zhong, Q.-Y. Yue, Q. Li, B.-Y. Gao, X. Xu, Removal of Cu(II) and Cr(VI) from wastewater by an amphoteric sorbent based on cellulose-rich biomass, Carbohydr. Polym., 111 (2014) 788–796.
[7] D.M. Stearns, L.J. Kennedy, K.D. Courtney, P.H. Giangrande, L.S. Phieffer, K.E. Wetterhahn, Reduction of chromium(VI) by ascorbate leads to chromium-DNA binding and DNA strand breaks in vitro, Biochemistry, 34 (1995) 910–919.
[8] S.J. Kwak, J.-C. Yoo, D.H. Moon, K. Baek, Role of clay minerals on reduction of Cr(VI), Geoderma, 312 (2018) 1–5.
[9] S. Ahmadzadeh, M. Yoosefian, M. Rezayi, Comprehensive experimental and theoretical investigations on chromium(III) trace detection in biological and environmental samples using polymeric membrane sensor, Int. J. Environ. Anal. Chem., 1 (2019) 1–16.
[10] S. Badakhshan, S. Ahmadzadeh, A. Mohseni-Bandpei, M. Aghasi, A. Basiri, Potentiometric sensor for iron(III) quantitative determination: experimental and computational approaches, BMC Chem., 13 (2019) 1–12, https://doi.org/10.1186/s13065-019-0648-x.
[11] M. Owlad, M.K. Aroua, W.A.W. Daud, S. Baroutian, Removal of hexavalent chromium-contaminated water and wastewater: a review, Water Air Soil Pollut., 200 (2009) 59–77.
[12] C.E. Barrera-Díaz, V. Lugo-Lugo, B. Bilyeu, A review of chemical, electrochemical and biological methods for aqueous Cr(VI) reduction, J. Hazard. Mater., 223 (2012) 1–12.
[13] P.Y. Jeon, M.-E. Lee, K. Baek, Adsorption and photocatalytic activity of biochar with graphitic carbon nitride (g-C_3N_4), J. Taiwan Inst. Chem. Eng., 77 (2017) 244–249.

[14] T. Wang, L.Y. Zhang, C.F. Li, W.C. Yang, T.T. Song, C.J. Tang, Y. Meng, S. Dai, H.Y. Wang, L.Y. Chai, Synthesis of core–shell magnetic Fe_3O_4@poly(*m*-phenylenediamine) particles for chromium reduction and adsorption, Environ. Sci. Technol., 49 (2015) 5654–5662.
[15] C.C. Wan, J. Li, Facile synthesis of well-dispersed superparamagnetic γ-Fe_2O_3 nanoparticles encapsulated in three-dimensional architectures of cellulose aerogels and their applications for Cr(VI) removal from contaminated water, ACS Sustainable Chem. Eng., 3 (2015) 2142–2152.
[16] R. Foroutan, R. Zareipour, R. Mohammadi, Fast adsorption of chromium(VI) ions from synthetic sewage using bentonite and bentonite/bio-coal composite: a comparative study, Mater. Res. Express, 6 (2018) 1–26.
[17] J.W. He, Y. Long, Y.Y. Wang, C.L. Wei, J.J. Zhan, Aerosol-assisted self-assembly of reticulated N-doped carbonaceous submicron spheres for effective removal of hexavalent chromium, ACS Appl. Mater. Interfaces, 8 (2016) 16699–16707.
[18] B. Qiu, C.X. Xu, D.Z. Sun, H. Yi, J. Guo, X. Zhang, H.L. Qu, M. Guerrero, X.F. Wang, N. Noel, Z.P. Luo, Z.H. Guo, S.Y. Wei, Polyaniline coated ethyl cellulose with improved hexavalent chromium removal, ACS Sustainable Chem. Eng., 2 (2014) 2070–2080.
[19] F. Wang, L.-Y. Liu, F. Liu, L.-G. Wang, T. Ouyang, C.-T. Chang, Facile one-step synthesis of magnetically modified biochar with enhanced removal capacity for hexavalent chromium from aqueous solution, J. Taiwan Inst. Chem. Eng., 81 (2017) 414–418.
[20] M.L. Cao, Y.F. Yu, Synthesis and characterization of montmorillonite inorgano-intercalation compound assisted by microwave irradiation, J. Wuhan Univ. Technol.-Mater. Sci. Ed., 25 (2010) 444–448.
[21] J. Lehmann, J. Gaunt, M. Rondon, Bio-char sequestration in terrestrial ecosystems – a review, Mitigation Adapt. Strategies Global Change, 11 (2006) 403–427.
[22] M. Ahmad, A.U. Rajapaksha, J.E. Lim, M. Zhang, N. Bolan, D. Mohan, M. Vithanage, S.S. Lee, Y.S. Ok, Biochar as a sorbent for contaminant management in soil and water: a review, Chemosphere, 99 (2014) 19–33.
[23] L. Beesley, M. Marmiroli, The immobilisation and retention of soluble arsenic, cadmium and zinc by biochar, Environ. Pollut., 159 (2011) 474–480.
[24] K.T. Klasson, L.H. Wartelle, J.E. Rodgers III, I.M. Lima, Copper(II) adsorption by activated carbons from pecan shells: effect of oxygen level during activation, Ind. Crops Prod., 30 (2009) 72–77.
[25] J.K. Sun, F. Lian, Z.Q. Liu, L.Y. Zhu, Z.G. Song, Biochars derived from various crop straws: characterization and Cd(II) removal potential, Ecotoxicol. Environ. Saf., 106 (2014) 226–231.
[26] M. Uchimiya, S.C. Chang, K.T. Klasson, Screening biochars for heavy metal retention in soil: role of oxygen functional groups, J. Hazard. Mater., 190 (2011) 432–441.
[27] C. Bilgiç, Investigation of the factors affecting organic cation adsorption on some silicate minerals, J. Colloid Interface Sci., 281 (2005) 33–38.
[28] H. Wang, L. Tan, B.W. Hu, M.Q. Qiu, L.P. Liang, L.F. Bao, Y.L. Zhu, G.H. Chen, C.C. Huang, Removal of Cr(VI) from acid mine drainage with clay-biochar composite, Desal. Water Treat., 165 (2019) 212–221.
[29] K. Chinoune, K. Bentaleb, Z. Bouberka, A. Nadim, U. Maschke, Adsorption of reactive dyes from aqueous solution by dirty bentonite, Appl. Clay Sci., 123 (2016) 64–75.
[30] Y. Yao, B. Gao, J. Fang, M. Zhang, H. Chen, Y.M. Zhou, A.E. Creamer, Y.N. Sun, L.Y. Yang, Characterization and environmental applications of clay–biochar composites, Chem. Eng. J., 242 (2014) 136–143.
[31] K. Kalantari, M.B. Ahmad, H.R.F. Masoumi, K. Shameli, M. Basri, R. Khandanlou, Rapid and high capacity adsorption of heavy metals by Fe_3O_4/montmorillonite nanocomposite using response surface methodology: preparation, characterization, optimization, equilibrium isotherms, and adsorption kinetics study, J. Taiwan Inst. Chem. Eng., 49 (2015) 192–198.
[32] J.W. Lin, B.H. Jiang, Y.H. Zhan, Effect of pre-treatment of bentonite with sodium and calcium ions on phosphate adsorption onto zirconium-modified bentonite, J. Environ. Manage., 217 (2018) 183–195.
[33] M.L. Jiang, H. Jin, C. Deng, S. Wang, Preparation and characterization of nanoparticles containing Fe_3O_4 cores in biochar, J. Agro-Environ. Sci., 37 (2018) 592–597.
[34] M. Segad, B. Jonsson, T. Åkesson, B. Cabane, Ca/Na montmorillonite: structure, forces and swelling properties, Langmuir, 26 (2010) 5782–5790.
[35] L.M. Zhou, H. Chen, X.H. Jiang, F. Lu, Y.F. Zhou, W.M. Yin, X.Y. Ji, Modification of montmorillonite surfaces using a novel class of cationic gemini surfactants, J. Colloid Interface Sci., 332 (2009) 16–21.
[36] S.F. Wang, Y. Hu, R.W. Zong, Y. Tang, Z.Y. Chen, W.C. Fan, Preparation and characterization of flame retardant ABS/montmorillonite nanocomposite, Appl. Clay Sci., 25 (2004) 49–55.
[37] F. Yang, S.S. Zhang, H.P. Li, S.S. Li, K. Cheng, J.-S. Li, D.C.W. Tsang, Corn straw-derived biochar impregnated with α-FeOOH nanorods for highly effective copper removal, Chem. Eng. J., 348 (2018) 191–201.
[38] E. Derakhshani, A. Naghizadeh, Optimization of humic acid removal by adsorption onto bentonite and montmorillonite nanoparticles, J. Mol. Liq., 259 (2018) 76–81.
[39] S. Ahmadzadeh, M. Dolatabadi, In situ generation of hydroxyl radical for efficient degradation of 2,4-dichlorophenol from aqueous solutions, Environ. Monit. Assess., 190 (2018) 340.
[40] R. Foroutan, R. Mohammadi, A.S. Adeleye, S. Farjadfard, Z. Esvandi, H. Arfaeinia, G.A. Sorial, B. Ramavandi, S. Sahebi, Efficient arsenic(V) removal from contaminated water using natural clay and clay composite adsorbents, Environ. Sci. Pollut. Res., 26 (2019) 29748–29762.
[41] M. Shafiee, R. Foroutan, K. Fouladi, M. Ahmadlouydarab, B. Ramavandi, S. Sahebi, Application of oak powder/Fe_3O_4 magnetic composite in toxic metals removal from aqueous solutions, Adv. Powder Technol., 30 (2018) 544–554.
[42] R. Saravanan, M.M. Khan, V.K. Gupta, E. Mosquera, F. Gracia, V. Narayanan, A. Stephen, ZnO/Ag/CdO nanocomposite for visible light-induced photocatalytic degradation of industrial textile effluents, J. Colloid Interface Sci., 452 (2015) 126–133.
[43] S. Ahmadzadeh, M. Dolatabadi, Electrochemical treatment of pharmaceutical wastewater through electrosynthesis of iron hydroxides for practical removal of metronidazole, Chemosphere, 212 (2018) 533–539.
[44] W.H. Zhang, S.Y. Mao, H. Chen, L. Huang, R.L. Qiu, Pb(II) and Cr(VI) sorption by biochars pyrolyzed from the municipal wastewater sludge under different heating conditions, Bioresour. Technol., 147 (2013) 545–552.
[45] T.M. Abdel-Fattah, M.E. Mahmoud, S.B. Ahmed, M.D. Huff, J.W. Lee, S. Kumar, Biochar from woody biomass for removing metal contaminants and carbon sequestration, J. Ind. Eng. Chem., 22 (2015) 103–109.
[46] L.-G. Yan, Y.-Y. Xu, H.-Q. Yu, X.-D. Xin, Q. Wei, B. Du, Adsorption of phosphate from aqueous solution by hydroxy-aluminum, hydroxy-iron and hydroxy-iron–aluminum pillared bentonites, J. Hazard. Mater., 179 (2010) 244–250.
[47] D.H. Park, Y.-S. Yun, J.M. Park, Reduction of hexavalent chromium with the brown seaweed *Ecklonia* biomass, Environ. Sci. Technol., 38 (2004) 4860–4864.
[48] M. Liang, S.P. Xu, Y.N. Zhu, X. Chen, Z.L. Deng, L.L. Yan, H.J. He, Preparation and characterization of Fe-Mn binary oxide/mulberry stem biochar composite adsorbent and adsorption of Cr(VI) from aqueous solution, Int. J. Environ. Res. Public Health, 17 (2020) 676, doi: 10.3390/ijerph17030676.
[49] T. Chen, Y.X. Zhang, H.T. Wang, W.J. Lu, Z.Y. Zhou, Y.C. Zhang, L.L. Ren, Influence of pyrolysis temperature on characteristics and heavy metal adsorptive performance of biochar derived from municipal sewage sludge, Bioresour. Technol., 164 (2014) 47–54.
[50] Y. Abshirini, R. Foroutan, H. Esmaeili, Cr(VI) removal from aqueous solution using activated carbon prepared from *Ziziphus spina–christi* leaf, Mater. Res. Express, 6 (2018) 1–37.